



Published in final edited form as:

Biometals. 2019 December ; 32(6): 951–964. doi:10.1007/s10534-019-00226-z.

Using FluoZin-3 and fura-2 to monitor acute accumulation of free intracellular Cd²⁺ in a pancreatic beta cell line

Latha M. Malaiyandi, Harsh Sharthiya, Ameir N. Barakat

Departments of Anatomy, College of Graduate Studies, Midwestern University, Downers Grove, IL 60515, USA

Joshua R. Edwards, Kirk E. Dineley

Departments of Pharmacology, College of Graduate Studies, Midwestern University, 555 31st Street, Downers Grove, IL 60515, USA

Abstract

The understanding of cellular Cd²⁺ accumulation and toxicity is hampered by a lack of fluorescent indicators selective for intracellular free Cd²⁺ ([Cd²⁺]_i). In this study, we used depolarized MIN6 mouse pancreatic beta cells as a model for evaluating [Cd²⁺]_i detection with commercially available fluorescent probes, most of which have been traditionally used to visualize [Ca²⁺]_i and [Zn²⁺]_i. We trialed a panel of 12 probes including fura-2, FluoZin-3, Leadmium Green, Rhod-5N, indo-1, Fluo-5N, and others. We found that the [Zn²⁺]_i probe FluoZin-3 and the traditional [Ca²⁺]_i probe fura-2 responded most consistently and robustly to [Cd²⁺]_i accumulation mediated by voltage-gated calcium channels. While selective detection of [Cd²⁺]_i by fura-2 required the omission of Ca²⁺ from extracellular buffers, FluoZin-3 responded to [Cd²⁺]_i similarly in the presence or absence of extracellular Ca²⁺. Furthermore, we showed that FluoZin-3 and fura-2 can be used together for simultaneous monitoring of [Ca²⁺]_i and [Cd²⁺]_i in the same cells. None of the other fluorophores tested were effective [Cd²⁺]_i detectors in this model.

Keywords

MIN6; Cadmium; Leadmium Green; Voltage-gated calcium channel; Metal toxicity

Open Access This article is distributed under the terms of the Creative Commons Attribution 4.0 International License (<http://creativecommons.org/licenses/by/4.0/>), which permits unrestricted use, distribution, and reproduction in any medium, provided you give appropriate credit to the original author(s) and the source, provide a link to the Creative Commons license, and indicate if changes were made.

K. E. Dineley, kdinel@midwestern.edu.

Present Address: H. Sharthiya, AbbVie Inc., Headquarters 1 N. Waukegan Road, North Chicago, IL 60064, USA

Author contributions KED and LMM conceived and coordinated the study, in consultation with JRE. ANB maintained and plated MIN6 cell cultures. LMM, KED, HS, and ANB performed and analyzed fluorescence microscopy experiments. LMM performed and analyzed spectrofluorimetric experiments. JRE coordinated ICP-MS measurements. LMM and KED wrote the initial manuscript draft, and all authors reviewed and approved the final version.

Conflict of interest The authors declare that they have no conflict of interest.

Publisher's Note Springer Nature remains neutral with regard to jurisdictional claims in published maps and institutional affiliations.

Introduction

Cadmium is a highly toxic trace metal with virtually no biological function. Human exposure to cadmium occurs via cigarette smoking, ingestion of contaminated foodstuffs, and occupational and environmental exposure (Nordberg 2009). Depending on the route of intake and the timeframe over which it occurs, cadmium can be particularly toxic to kidney, liver, GI, bone, lung, and reproductive tissues. Some data suggest that cadmium may also be associated with pancreatic cancer and type II diabetes (Muayed et al. 2012; Edwards and Ackerman 2016; Djordjevic et al. 2019). Accordingly, the U.S. Agency for Toxic Substances and Disease Registry currently ranks cadmium 7th out of 275 environmental hazardous substances (ATSDR 2019). At the cellular level, Cd^{2+} toxicity is only partly understood. Intracellular accumulation can occur through a variety of pathways normally used by Ca^{2+} , Zn^{2+} , and other metals (Thévenod 2010; Bouron et al. 2014). Once inside the cell, the deleterious effects of Cd^{2+} probably result from its tendency to displace other biologically important metals from critical proteins, in a process that is referred to as ionic mimicry (Bridges and Zalups 2005).

One major limitation to our understanding of cadmium toxicity is a lack of fluorophores that are selective for intracellular free Cd^{2+} ($[\text{Cd}^{2+}]_i$) and are easy to use. The first live cell studies of $[\text{Cd}^{2+}]_i$ uptake appropriated the iconic Ca^{2+} probe fura-2, which also has extremely high affinity for Cd^{2+} (Hinkle et al. 1992). Those experiments were often performed in Ca^{2+} -free solutions in order to minimize any Ca^{2+} contribution to the intracellular signal. More recently, the Cd^{2+} - and Pb^{2+} -sensitive probe Leadmium Green has aided the study of $[\text{Cd}^{2+}]_i$ handling in a variety of organisms including plants (Zanella et al. 2015; Greger et al. 2016), mammals (Romero et al. 2009; Miura et al. 2013), and microbes (Manzano et al. 2013; Johnson et al. 2018, 2019). The high-affinity Zn^{2+} sensor FluoZin-3 is also responsive to Cd^{2+} (Zhao et al. 2009), and this promiscuity has been exploited to monitor $[\text{Cd}^{2+}]_i$ uptake in marine invertebrates (Ortega et al. 2017a, b) and rodent hippocampal slices (Kay and Rumschik 2011). Several other small chemical ion sensors have demonstrated Cd^{2+} sensitivity in cell-free conditions, including FluoZin-1 (Lee et al. 2005), Rhod-5N (Soibinet et al. 2008), indo-1 (Vo-Dinh et al. 1994), fura-2FF, and mag-fura-2 (Hyrč et al. 2000), but there is little or no data regarding their value in live-cell Cd^{2+} applications. Various laboratories have invented chemical and protein-based probes intended primarily for the detection of Cd^{2+} , several of which demonstrated potential to selectively report Cd^{2+} amidst Zn^{2+} and other competing metals, but none of these prototypes has yet been adopted into common use for the live-cell imaging of $[\text{Cd}^{2+}]_i$ (Vinkenborg et al. 2011; Chiu et al. 2013; Taki 2013).

In this study we evaluated a panel of fluorescent probes for their ability to monitor $[\text{Cd}^{2+}]_i$ in a model of acute accumulation. We limited our consideration to fluorophores that are commercially available, because they are easily procured by labs with modest resources, and their properties tend to be fairly well documented in the literature. $[\text{Cd}^{2+}]_i$ uptake was assayed in depolarized mouse insulinoma cells (MIN6), which express much of the machinery important to pancreatic beta cell function, including L-type voltage-gated Ca^{2+} channels that are readily activated with high extracellular potassium (Zhou et al. 2014). Of the 12 probes we tested, the high affinity Zn^{2+} indicator FluoZin-3 and the classic Ca^{2+}

probe fura-2 proved most useful as $[Ca^{2+}]_i$ detectors. We then conducted a series of experiments that compared the strengths and weaknesses of these two probes, including a dual dye method that uses both for the simultaneous monitoring of $[Cd^{2+}]_i$ and $[Ca^{2+}]_i$ inside the same cells.

Materials and methods

Reagents

Cell culture media, N,N,N',N'-tetrakis (2-pyridylmethyl) ethylenediamine (TPEN), and fluorescent probes (Calcium Green-5N, Fluo-5N, FluoZin-1, FluoZin-2, FluoZin-3, fura-2, indo-1, Leadmium Green, mag-fura-2, Newport Green DCF, and Rhod-5N) were purchased from Thermo Fisher Scientific. Fura-2FF was purchased from TEF Labs. Fetal bovine serum was purchased from Midwest Scientific. All other reagents were purchased from Sigma-Aldrich unless otherwise noted.

Cell culture

The mouse insulinoma cell line (MIN6) was generously provided by Dr. Malek El Muayed at Northwestern University, Feinberg School of Medicine and maintained according to previously published methods (Muayed et al. 2012). Briefly, cells were grown in high glucose Dulbecco's Modified Eagle's Medium (DMEM, Gibco #12430-054) supplemented with 0.1% 2-mercaptoethanol, 15% heat-inactivated fetal bovine serum and 1% penicillin/streptomycin (Sigma #P4333) at 37 °C and 5% CO₂. Round glass coverslips (18 mm, Warner Instruments) were coated with poly-L-lysine (Sigma #P4707) according to the manufacturer's recommended protocol, and trypsinized cells were plated at a density of 100,000 cells per coverslip placed in 12-well culture plates. Media was changed every 2 days, and cells were used 5–7 days following plating. Cells from passages 23–42 were used in experiments.

Epifluorescence microscopy

Live-cell fluorescence microscopy was carried out in a HEPES-buffered, phosphate-free salt solution (HBSS) containing (in mM): 137 NaCl, 5 KCl, 10 NaHCO₃, 0.9 MgSO₄, 1.4 CaCl₂, 20 HEPES, and 5.5 glucose, pH adjusted to 7.4 with NaOH. Depolarization was achieved with a high KCl, phosphate-free buffer containing (in mM): 92 NaCl, 50 KCl, 10 NaHCO₃, 0.9 MgSO₄, 1.4 CaCl₂, 20 HEPES, and 5.5 glucose, pH adjusted to 7.4 with NaOH. For nominally Ca²⁺-free experiments, CaCl₂ was omitted from both the HBSS and high KCl buffer. For loading of dye, cells were incubated for 30 min at room temperature in 500 μL loading buffer comprised of HBSS supplemented with 5 μM acetoxymethyl (AM) form of the fluorescent probe and bovine serum albumin (5 mg/mL). Coverslips with dye-loaded cells were placed in a 500 μL perfusion chamber and mounted on the microscope stage. The chamber was superfused at 5 mL/min with CaCl₂, CdCl₂, ZnSO₄, sodium pyruvate, MnCl₂, TPEN, and/or Ca²⁺ channel blockers at the indicated concentrations.

Live-cell microscopy of single dye experiments were performed at room temperature on an IX70 Olympus fluorescence microscope equipped with a 40× oil-immersion objective (UAPO/340, ND = 1.35). Excitation light was produced by a xenon lamp-based Lambda LS

stand-alone illuminator with filter wheels (Sutter Instruments). Optics for fura-2, fura-2FF and mag-fura-2 used alternately switched 340/20 and 380/11 nm excitation filters, 400 nm dichromatic mirror, and 510/84 nm emission filter. Optics for indo-1 used 340/10 nm excitation filter, 387 nm dichromatic mirror, and alternately switched 405/30 and 485/25 nm emission filters. For Calcium Green-5N, Fluo-5N, FluoZin-1, FluoZin-2, FluoZin-3, Leadmium Green, and Newport Green DCF: 480/20 nm excitation filter; 500 nm dichromatic mirror; and 520 nm emission filter. For Rhod-5N: 540/20 nm excitation filter; 570 nm dichromatic mirror, and 590 nm emission filter. Images were captured with an LT Flash4.0 CMOS camera with HCIImage acquisition software (Hamamatsu Photonics).

Dual dye experiments using fura-2 and FluoZin-3 were performed on a Nikon Eclipse TE2000-S fluorescence microscope equipped with a 40× oil-immersion objective (S FLUOR, ND = 1.30), illuminated by a xenon lamp-based Lambda DG-4 high speed filter changer (Sutter Instruments). Cells were incubated in loading buffer supplemented with 5 μM fura-2 and FluoZin-3 for 45 min at room temperature. For fura-2, excitation light was modified by alternately switched 340/11 and 380/11 nm excitation filters. For FluoZin-3, light was modified by a 495/10 nm excitation filter. A 510 nm dichromatic mirror and 560/80 emission filter were used for both dyes. The camera and software were the same types used in the Olympus system described above.

Spectrofluorimetry

Spectrofluorimetric measurements of the tetrapotassium salt form of FluoZin-3 were performed on a Perkin Elmer Enspire multimode plate reader. Fluorescence was recorded from 96-well black plates with 495 nm excitation and 517 nm emission. Experiments were performed in Chelex 100-treated buffer containing (in mM): 140 KCl, 10 MOPS, 10 nitrilotriacetic acid (NTA), pH 7. FluoZin-3 salt was added at a final concentration of 500 nM, and serial dilutions of metal from 1000 × stock solutions of CdCl₂ or ZnSO₄ were added in the range of 0–9 mM, to a final well volume of 100 μL. Free metal concentrations were calculated using the Maxchelator program (<https://somapp.ucdmc.ucdavis.edu/pharmacology/bers/maxchelator/webmaxc/webmaxcS.htm>). Data were represented as a percentage of fluorescence at baseline (50 μM TPEN) versus log of free metal (in M). K_D values were calculated by curve-fitting the data using nonlinear regression of one-site specific binding with B_{max} constrained between 0 and 100.

Inductively coupled plasma mass spectrometry (ICP-MS)

Total intracellular Cd²⁺ levels were measured by inductively coupled plasma mass spectrometry (ICP-MS) in samples sent to the Michigan State University Veterinary Diagnostic Laboratory. MIN6 cells were plated in 12-well plates coated with poly-L-lysine and maintained in growth media for 5–7 days. All HBSS buffers were made nominally Ca²⁺-free. Cells were rinsed twice in non-depolarizing HBSS, then treated with 0, 30 or 300 μM CdCl₂ in 2 mL volume of depolarizing HBSS for 5 minutes. Other wells were treated with 30 μM CdCl₂ in non-depolarizing HBSS. Plates were placed on a rocker during the 5-minute treatment to simulate bath perfusion use in the microscopy experiments. Cells were rinsed three times in non-depolarizing HBSS containing 100 μM EDTA to remove any extracellular bound Cd²⁺, followed by a final rinse in non-depolarizing HBSS. Cells were lysed using 0.1

mL commercially available lysing buffer (Thermo Fisher Scientific 78505). For each trial, cell lysates were pooled from three wells and experiments were repeated in at least three different cell culture passages.

Statistical analysis

Statistical analyses and graphical representations of data were performed with GraphPad Prism 8.1 software. For the fura dyes, the ratio was calculated as the background-subtracted signal at 340 nm divided by the background-subtracted signal at 380 nm. For indo-1, the ratio was similarly calculated as the background-subtracted signal at 405 nm divided by the background subtracted signal at 485 nm. For single wavelength dyes, fluorescence signal (F) was divided by the starting fluorescence value (F_0), after background-subtraction. For a given coverslip, fluorescence was typically collected from a field of 30–60 cells. Representative data traces are plotted as an averaged fluorescence change from all cells within a field from one coverslip. Summary data are presented in bar graphs as mean \pm SD consisting of four to six coverslips for each condition, using cells from at least three different cell culture preparations. Where appropriate, statistical analyses used Welch's t-test or ANOVA with Tukey's post hoc test for multiple comparisons. Statistical significance was determined as $p < 0.05$.

Results

Our standard stimulus for provoking $[Cd^{2+}]_i$ accumulation in MIN6 cells used HBSS buffer containing 50 mM KCl and supplemented with 30 μ M $CdCl_2$, applied for 5 minutes. This triggers rapid depolarization, activation of voltage-gated Ca^{2+} channels, and Cd^{2+} influx. Of the assortment of small molecule ratiometric and single wavelength probes that are potentially useful as live-cell Cd^{2+} sensors, only two that we tested, fura-2 and FluoZin-3, responded to $[Cd^{2+}]_i$ accumulation in consistent and robust fashion (mean fura-2 ratio change = 1.58; mean FluoZin-3 F/F_0 change = 3.78; Fig. 1). The fluorescence micrographs show dye signal that is for the most part evenly distributed throughout the cell, indicating minimal compartmentalization of metal or probe. All of our subsequent experiments focused on fura-2 and Fluo-Zin-3.

We next examined more carefully the utility of fura-2 in our model by comparing the signal characteristics associated with $[Cd^{2+}]_i$ and $[Ca^{2+}]_i$ accumulation. Figure 2a shows a typical fura-2 depolarization response in an excitable cell, under conditions where extracellular Ca^{2+} is abundant. Notable features included a fast, robust rise in signal that declined quickly to a secondary plateau, which then decayed slowly over the duration of the depolarizing stimulus. Termination of depolarization was sufficient to permit the signal to return quickly and nearly completely to starting values. Figure 2b shows the fura-2 response to $[Cd^{2+}]_i$ accumulation (30 μ M extracellular Cd^{2+}) when Ca^{2+} is omitted from the buffer. In contrast to the kinetics of the $[Ca^{2+}]_i$ signal, the $[Cd^{2+}]_i$ rise was much more gradual and remained elevated after depolarization was finished. Restoration of baseline fluorescence did not occur spontaneously but instead required application of the membrane-permeant, heavy metal chelator TPEN (50 μ M). We confirmed that L-type voltage-gated Ca^{2+} channels (VGCCs) are a major route of accumulation for both ions under these circumstances. The standard L-

type blockers nifedipine, nitrendipine, and verapamil inhibited fura-2 responses as much as 89% for $[Ca^{2+}]_i$ and 77% for $[Cd^{2+}]_i$ (Fig. 2c). The fura-2 response to $[Cd^{2+}]_i$ proved to be concentration-dependent across values tested up to 300 μM extracellular Cd^{2+} , and 10 μM extracellular Cd^{2+} was the apparent lower limit for delivering enough intracellular Cd^{2+} to produce a perceptible fura-2 response (Figs. 3a, b). These results were supported by ICP-MS measurements of whole cell cadmium (Fig. 3c), which show that depolarization increased cellular cadmium content, and that intracellular cadmium accumulation was broadly proportional to extracellular Cd^{2+} .

Up to this point, the $[Cd^{2+}]_i$ trials were all performed in the absence of any added Ca^{2+} (i.e. nominally Ca^{2+} -free buffer). While this tactic helps to minimize signal confounds that are expected when exploiting a high-affinity $[Ca^{2+}]_i$ probe for the detection of $[Cd^{2+}]_i$, it diminishes the physiological relevance of these experiments. In Fig. 4, we explored how fura-2 detection of $[Cd^{2+}]_i$ changes over a range of extracellular Ca^{2+} concentrations. When extracellular Ca^{2+} is absent or minimal (Fig. 4a–c), the fura-2 response is dominated by $[Cd^{2+}]_i$, as shown by the slow and continuous rise, and TPEN reversal. At 0.6 mM extracellular Ca^{2+} (Fig. 4d), the signal became embellished with a swift rise that began immediately upon depolarization, which was further enhanced when extracellular Ca^{2+} was restored to physiologic levels (1.4 mM, Fig. 4e). The rapid initial response was followed by a secondary phase where the signal climbed slowly but continuously for the duration of the depolarizing stimulus. Presumably, this secondary rise reflects the gradual accumulation of $[Cd^{2+}]_i$ in cells that already have elevated $[Ca^{2+}]_i$. Thus, the trace in Fig. 4e can be viewed as a hybrid product of the traces obtained in Fig. 4a and 4f with Cd^{2+} or Ca^{2+} alone, respectively.

These data demonstrate that fura-2 can be used to monitor $[Cd^{2+}]_i$ with reasonable sensitivity, provided that extracellular Ca^{2+} is scarce. Yet even in the presence of physiological extracellular Ca^{2+} , the component contribution of each ion can be perceived in the fura-2 recording. Still, because it is not possible to precisely dissect the two signals, the practical use of fura-2 in this context is limited. FluoZin-3 is a single wavelength Zn^{2+} indicator, that is insensitive to Ca^{2+} , but showed promise as an $[Cd^{2+}]_i$ sensor in our pilot assays (Fig. 1). Throughout a series of depolarization trials in 1.4 mM $CaCl_2$, FluoZin-3 responded to $[Cd^{2+}]_i$ in concentration-dependent fashion, with F/F_0 increasing by roughly 11-fold (Fig. 5a, b). The gradual rise of FluoZin-3 was kinetically consistent with the $[Cd^{2+}]_i$ -induced fura-2 changes observed in Fig. 3a. In contrast to fura-2 however, the presence or absence of extracellular Ca^{2+} did not alter the FluoZin-3 response to the Cd^{2+} challenge, suggesting that $[Ca^{2+}]_i$ accumulation does not meaningfully confound the FluoZin-3 response to $[Cd^{2+}]_i$. We noted that Ca^{2+} influx alone (i.e. depolarization in the presence of 1.4 mM $CaCl_2$, without added Cd^{2+}) stimulated a small but consistent FluoZin-3 increase (about 1.5-fold). This was prevented by co-treatment with TPEN (data not shown), suggesting that Ca^{2+} influx mobilized a small amount of intracellular Zn^{2+} , which is consistent with previous reports that documented Ca^{2+} -induced Zn^{2+} mobilization in other cell types (Dineley et al. 2008; Li et al. 2011; Duncan et al. 2016). For comparative purposes, we also conducted FluoZin-3 trials with depolarization-induced Zn^{2+} influx (Fig. 6). In nominally Ca^{2+} -free conditions, the signal elicited by 30 μM Zn^{2+} was similar to that obtained with 30 μM Cd^{2+} (Fig. 6a, b). In contrast to $[Cd^{2+}]_i$ however, FluoZin-3 reporting

of $[Zn^{2+}]_i$ was markedly reduced in the presence of 1.4 mM $CaCl_2$. This suggests that Zn^{2+} , unlike Cd^{2+} , is a rather poor competitor for Ca^{2+} permeable pathways, under depolarizing circumstances when Ca^{2+} is abundant. The FluoZin-3 responses were also reduced by approximately 80% for Zn^{2+} and 92% for Cd^{2+} with VGCC blockers (Fig. 6c). It is important to note that equivalent intracellular fluorescence does not necessarily indicate equivalent amounts of intracellular metal. Determination of FluoZin-3 affinities yielded dissociation constants of 3.67 nM for Zn^{2+} , and 129 nM for Cd^{2+} (Fig. 6d)—values that are broadly consistent with previous publications. This difference in affinities and also, possibly, in quantum yields and other factors means that a much smaller concentration of Zn-FluoZin-3 could potentially produce the same fluorescence intensity as a much larger amount of Cd-FluoZin-3.

The spectral compatibility of fura-type probes with FluoZin-3 allows both dyes to be surveyed simultaneously with basic live-cell imaging equipment (Devinney et al. 2005). This, combined with the facts that FluoZin-3 responds well to Cd^{2+} but is insensitive to Ca^{2+} , and that fura-2 responds very well to Ca^{2+} , suggested that both dyes could be used together for concurrent detection of $[Cd^{2+}]_i$ and $[Ca^{2+}]_i$. Figure 7a shows a dual dye approach to simultaneous monitoring of intracellular Cd^{2+} and Ca^{2+} in depolarized MIN6 cells. The results are approximately similar to those obtained by using the dyes individually, however the FluoZin-3 signal is somewhat suppressed, compared to the analogous 30 μ M Cd^{2+} trial in Fig. 5. This is surely due to some fraction of the $[Cd^{2+}]_i$ load interacting with fura-2 instead of FluoZin-3. Nevertheless, a robust and consistent FluoZin-3 response was obtained. Because these same principles can be applied to the simultaneous detection of $[Zn^{2+}]_i$ and $[Ca^{2+}]_i$, we then tested the dual dye approach with 30 μ M $ZnSO_4$ and 1.4 mM $CaCl_2$, under depolarizing conditions. In this paradigm, FluoZin-3 yielded a paltry response, while the fura-2 response was rapid and robust, which is consistent with the limited $[Zn^{2+}]_i$ accumulation observed with FluoZin-3, in the presence of extracellular Ca^{2+} , in Fig. 5b. Another important observation reinforced by these trials is the lack of fura-2 recovery associated with $[Cd^{2+}]_i$ accumulation. This contrasts with the $[Zn^{2+}]_i$ trials, where a short rinse was sufficient to return the fura-2 signal to pre-stimulus values. However, under circumstances of $[Cd^{2+}]_i$ accumulation, both dye signals remained elevated, until TPEN was applied. The impact of $[Cd^{2+}]_i$ on intracellular transport processes is largely unknown, however it is reasonable to assume that elevated $[Ca^{2+}]_i$ persists because $[Cd^{2+}]_i$ disrupts $[Ca^{2+}]_i$ clearance mechanisms (Biagioli et al. 2008). Fluorescence micrographs in Fig. 7d–k present pseudocolored, three-part composite images that assign the 340 nm fura-2 signal to the red channel, 380 nm fura-2 signal to the green channel, and 490 nm FluoZin-3 signal to the blue channel. The images were taken roughly at the time points indicated in Fig. 7a, b.

The abundance of intracellular Zn^{2+} binding sites that also have high affinity for Cd^{2+} raises the possibility of Cd^{2+} -induced mobilization of intracellular Zn^{2+} . In that scenario, $[Zn^{2+}]_i$ could contribute importantly to the dye signals we have attributed to $[Cd^{2+}]_i$. Because there exists no live-cell probe that is sensitive to Cd^{2+} but insensitive to Zn^{2+} , this question cannot be answered conclusively. However, in a series of experiments that closely examines the fura-2 responses to $[Zn^{2+}]_i$ or $[Cd^{2+}]_i$, our data suggests that Cd^{2+} is the dominant free species inside the cell after depolarization-induced $[Cd^{2+}]_i$ accumulation, while $[Zn^{2+}]_i$ makes little if any contribution to the dye signal. In Fig. 8, cells were loaded with Zn^{2+} (0, 1,

and 10 μM) using the ionophore sodium pyrithione (Fig. 8a), or with Cd^{2+} (30, 100, and 300 μM) using depolarization (Fig. 8b) in order to achieve a maximum dye response for each metal. For Zn^{2+} , the ratio rose by 1.61 ± 0.06 ratio units (Fig. 8a), compared to 6.21 ± 1.01 units for Cd^{2+} (Fig. 8b). This shows that fura-2 can discriminate $[\text{Cd}^{2+}]_i$ from $[\text{Zn}^{2+}]_i$, based on the much greater dynamic range of ratio that is attained with $[\text{Cd}^{2+}]_i$. We then used this difference to determine which metal dominates the dye response in a paradigm where cells are loaded with both metals sequentially. Again using sodium pyrithione, we achieved high $[\text{Zn}^{2+}]_i$, then followed with Cd^{2+} under depolarization conditions (Fig. 8c). The initial Zn^{2+} challenge produced a peak ratio similar to the values obtained in Fig. 8a. The subsequent $[\text{Cd}^{2+}]_i$ load then further elevated the ratio beyond the $[\text{Zn}^{2+}]_i$ plateau. But when the sequence was reversed (Fig. 8d), a $[\text{Zn}^{2+}]_i$ load had little effect on a fura-2 response already dominated by $[\text{Cd}^{2+}]_i$. These data indicate that fura-2 favors $[\text{Cd}^{2+}]_i$ when both metals are present. Lastly, we examined the ability of $[\text{Mn}^{2+}]_i$ to quench fura-2 signals elicited by more modest metal loads (Fig. 8e, f). We hypothesized that, due to fura-2's significantly higher affinity for Cd^{2+} compared to Zn^{2+} ($K_D \sim 10^{-12}$ vs. $\sim 10^{-9}\text{M}$, respectively), the rate of Mn^{2+} quench would be slower for a signal dominated by $[\text{Cd}^{2+}]_i$. Conversely, if the "[$\text{Cd}^{2+}]_i$ response" was actually due to $[\text{Zn}^{2+}]_i$ that was displaced by Cd^{2+} , then the quenching kinetics in the Cd^{2+} trial would not differ from the Zn^{2+} trial. Our data show that $[\text{Mn}^{2+}]_i$ extinguished the 340 nm component of the $[\text{Cd}^{2+}]_i$ signal at a rate slower than a corresponding $[\text{Zn}^{2+}]_i$ signal (quenching rate for $[\text{Cd}^{2+}]_i$, in counts per minute, -8.61 ± 0.64 counts/min; for $[\text{Zn}^{2+}]_i$ -9.89 ± 0.77), in cells depolarized in the presence of 50 μM Zn^{2+} or Cd^{2+} . When considered as a whole, the data in Fig. 8 suggest that the intracellular $[\text{Cd}^{2+}]_i$ loads achieved in our model behave as free Cd^{2+} that interacts directly with the dye. It remains possible that some Zn^{2+} is liberated from intracellular binding sites, but this appears to be minimal.

Discussion

Our data provide a thorough comparison of probes that might be used for live-cell $[\text{Cd}^{2+}]_i$ detection in models of acute $[\text{Cd}^{2+}]_i$ accumulation. FluoZin-3 demonstrated several strengths in this context: it proved sensitive, it responded strongly across a range of Cd^{2+} concentrations, and its performance was not obviously altered by $[\text{Ca}^{2+}]_i$ changes. This last property lends FluoZin-3 a clear advantage over fura-2. Other convenient features of FluoZin-3 include single wavelength excitation and emission parameters that are common to many "green" probes, so it can be imaged with standard epifluorescence equipment, or with a 488 nm confocal laser. However, FluoZin-3 offers none of the potential benefits of ratiometric imaging, because its spectral maxima do not change with metal binding, and they remain at the same wavelengths regardless of the partnered metal. Also, there is the difficult question of $[\text{Zn}^{2+}]_i$ contribution to the $[\text{Cd}^{2+}]_i$ signal, which we consider at length in the paragraphs further below.

The utility of fura-2 as a $[\text{Cd}^{2+}]_i$ detector was established in a landmark study identifying L-type VGCCs as a potential route of intracellular Cd^{2+} accumulation (Hinkle et al. 1992). Subsequent work used fura-2 to identify Ca^{2+} -permeable pathways as routes of Cd^{2+} uptake in various cell types including cerebellar neurons (Usai et al. 1999), lymphoma cells (Li et al. 2000), melanotrophs (Shibuya and Douglas 1992), and pheochromocytoma cells (Hinkle

and Osborne 1994). A major limitation common to all those experiments was the need to leave Ca^{2+} out of the extracellular solutions, in order to minimize $[\text{Ca}^{2+}]_i$ contribution to the fura-2 signal. This complication is highlighted in our data, which show a fura-2 response to $[\text{Cd}^{2+}]_i$ that is progressively distorted as higher amounts of Ca^{2+} are added back into the extracellular solution. At physiological extracellular Ca^{2+} (1.4 mM), the resulting $[\text{Ca}^{2+}]_i$ load clearly becomes an important component of the fura-2 signal. Because fura-2 affinity for Cd^{2+} ($K_D \sim 10^{-12}\text{M}$) is about five orders of magnitude higher than for Ca^{2+} ($K_D \sim 10^{-7}\text{M}$) the ability of $[\text{Ca}^{2+}]_i$ to interfere with the $[\text{Cd}^{2+}]_i$ response is perhaps counterintuitive. However, here it is necessary to remember that methods using passive dye loading of AM esters can achieve very high intracellular dye concentrations—hundreds of micromolar, possibly even millimolar. In such conditions, the binding reaction is more a function of reactant concentrations, while the K_D becomes less important (Dineley et al. 2002). This explains in part how a large $[\text{Ca}^{2+}]_i$ burden might occupy a significant fraction of the available fura-2, in the presence of a much smaller amount of $[\text{Cd}^{2+}]_i$. The difficulty in distinguishing $[\text{Cd}^{2+}]_i$ amidst $[\text{Ca}^{2+}]_i$ is further complicated by the fact that the emission profile for both metals is essentially the same, making it impossible to resolve $[\text{Ca}^{2+}]_i$ from $[\text{Cd}^{2+}]_i$ based on the fura-2 emission maximum, isosbestic point, or other spectral properties. Nevertheless, fura-2 can be an effective live cell $[\text{Cd}^{2+}]_i$ sensor in circumstances where measures are taken to limit $[\text{Ca}^{2+}]_i$ changes. Furthermore, and in contrast to FluoZin-3, the ratiometric capabilities of fura-2 afford some protection against signal artifacts that arise from variable dye loading, photobleaching, and focus drift, all of which complicate the use of single wavelength probes, particularly in applications where the change from baseline is expected to be small.

The abundance of intracellular Zn^{2+} binding proteins that also possess high affinity for Cd^{2+} raises the possibility that $[\text{Zn}^{2+}]_i$ that is displaced by Cd^{2+} contributes importantly to the dye signals that we have attributed to $[\text{Cd}^{2+}]_i$. With respect to fura-2, we presented several lines of evidence (Fig. 8) suggesting that $[\text{Cd}^{2+}]_i$ is the major binding partner. The dynamic range of fura-2 proved to be several times greater for $[\text{Cd}^{2+}]_i$ compared to $[\text{Zn}^{2+}]_i$, and we used that difference in apparent efficacies to reveal that $[\text{Cd}^{2+}]_i$ outcompetes $[\text{Zn}^{2+}]_i$ in circumstances where both metals are abundant. Furthermore, in trials involving more modest metal accumulation, Mn^{2+} quenching of fura-2 was slower after $[\text{Cd}^{2+}]_i$, compared to $[\text{Zn}^{2+}]_i$. The simplest interpretation of these data suggests that Cd^{2+} is the major free species, while liberated Zn^{2+} appears to be minimal. Yet it remains possible that substantial $[\text{Zn}^{2+}]_i$ is mobilized and furthermore that it might be better reflected in the FluoZin-3 traces. Unfortunately, there is no practical way to discern any $[\text{Zn}^{2+}]_i$ component within a $[\text{Cd}^{2+}]_i$ -induced FluoZin-3 signal. The fixed spectral character of FluoZin-3 does not permit nuanced interrogation with different metals, and FluoZin-3 has no good quenching partners in live cell applications. Cu^{2+} is the only potent and effective quencher of FluoZin-3 (Zhao et al. 2009), but it is not useful in this context due to its inherent redox lability and poor membrane permeation. Finally, the viability of the quenching approach with fura-2 is facilitated by its extremely high Cd^{2+} affinity, which exceeds the Zn^{2+} affinity by three orders of magnitude. Whereas with FluoZin-3, Zn^{2+} and Cd^{2+} affinities are separated by a factor of only 10–30 fold—an actually modest difference that would be hard to practically exploit in live-cell imaging. The upshot is that no trick exists for discerning a $[\text{Zn}^{2+}]_i$

contribution to a FluoZin-3 response triggered by $[Cd^{2+}]_i$. A more informative consideration of the general question of Cd^{2+} -induced release of intracellular Zn^{2+} awaits the invention of a live-cell probe that is sensitive to one of these metals but not the other.

The combination of fura-2 and FluoZin-3 offers a potentially useful approach for studying the relationship between $[Cd^{2+}]_i$ and $[Ca^{2+}]_i$. Again, considering only their respective affinities it seems surprising that FluoZin-3 ($K_D Cd^{2+} \sim 10^{-7}$ M), could effectively compete for Cd^{2+} in the presence of fura-2 ($K_D Cd^{2+} \sim 10^{-12}$ M). This seeming paradox is perhaps explained by competitive binding dynamics, where a surfeit of $[Ca^{2+}]_i$ consumes much of the fura-2 binding capacity, leaving $[Cd^{2+}]_i$ free to bind with FluoZin-3.

In the current study, we were most surprised by the nearly complete failure of Leadmium Green to respond to $[Cd^{2+}]_i$. Other groups have used Leadmium Green to report Cd^{2+} uptake in various plant and animal systems (Miura et al. 2013; Greger et al. 2016; Johnson et al. 2018, 2019). Our own prior work with a mouse hippocampal cell line concluded that Leadmium Green is a reliable $[Cd^{2+}]_i$ sensor, so long as any concomitant $[Zn^{2+}]_i$ perturbations are kept minimal (Malaiyandi et al. 2016). However, Leadmium Green did not respond to depolarization-induced $[Cd^{2+}]_i$ accumulation in the MIN6 cells used in the present study. The inconsistency between our current and previous data might be explained by the different methods used to deliver $[Cd^{2+}]_i$; the previous work used the ionophore pyrithione, which probably introduces a much larger $[Cd^{2+}]_i$ burden compared to what can be achieved via activation of endogenous ion channels. Other probes we evaluated, e.g. indo-1, Rhod-5N, mag-fura-2, etc., had shown promise in cell-free systems (Vo-Dinh et al. 1994; Hyrc et al. 2000; Soibinet et al. 2008; Johnson 2010). But when applied to our MIN6 cell model of $[Cd^{2+}]_i$ accumulation, none of them proved effective as live cell $[Cd^{2+}]_i$ sensors. These results underscore the inherent difficulties in translating in vitro Cd^{2+} responsiveness into practical utility inside the living cell.

Conclusion

In this study we have carefully evaluated a collection of commercially available Cd^{2+} -sensitive fluorophores for their utility as $[Cd^{2+}]_i$ probes. FluoZin-3 and fura-2 proved most effective, but care must be taken to assure that their signals are not confounded by $[Zn^{2+}]_i$ or $[Ca^{2+}]_i$, respectively. The combination of FluoZin-3 and fura-2 offers a novel method for the simultaneous detection of $[Cd^{2+}]_i$ and $[Ca^{2+}]_i$.

Acknowledgements

We extend thanks to Alice Meyer for preparing MIN6 cultures, Iga Fudyma for assistance with data analysis, and Peter Lamar for proofreading.

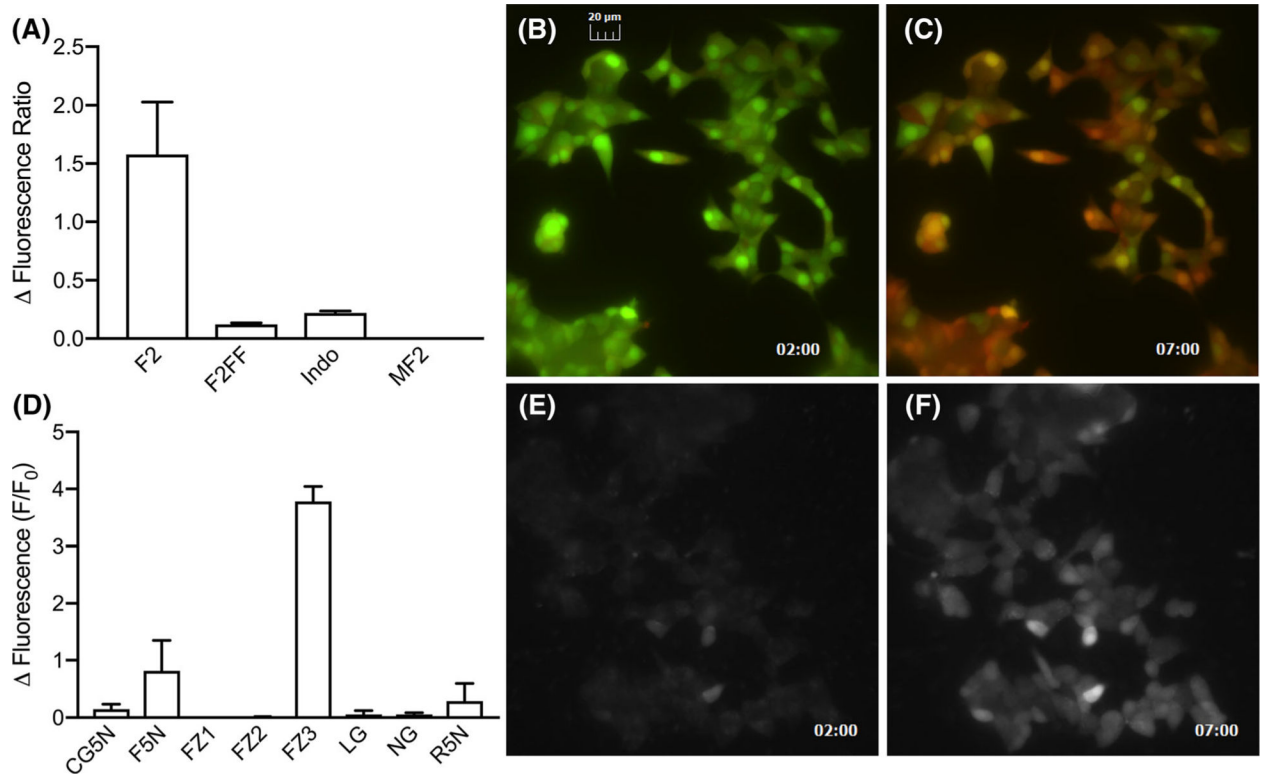
Funding This work was supported by the National Institutes of Health (R15ES028443) and intramural funds from Midwestern University. The funding sources had no involvement in study design; in the collection, analysis and interpretation of data; in the writing of the report; or in the decision to submit the article for publication.

References

ATSDR's Substance Priority List. Division of toxicology and human health sciences <https://www.atsdr.cdc.gov/spl/index.html#2017spl>. Accessed 18 July 2019

- Biagioli M, Pifferi S, Raghianti M et al. (2008) Endoplasmic reticulum stress and alteration in calcium homeostasis are involved in cadmium-induced apoptosis. *Cell Calcium* 43:184–195. 10.1016/j.ceca.2007.05.003 [PubMed: 17588656]
- Bouron A, Kiselyov K, Oberwinkler J (2014) Permeation, regulation and control of expression of TRP channels by trace metal ions. *Pflug Arch* 467:1143–1164. 10.1007/s00424-014-1590-3
- Bridges CC, Zalups RK (2005) Molecular and ionic mimicry and the transport of toxic metals. *Toxicol Appl Pharmacol* 204:274–308. 10.1016/j.taap.2004.09.007 [PubMed: 15845419]
- Chiu T-Y, Chen P-H, Chang C-L, Yang D-M (2013) Live-cell dynamic sensing of Cd(2⁺) with a FRET-based indicator. *PLoS ONE* 8:e65853 10.1371/journal.pone.0065853 [PubMed: 23776557]
- Devinney MJ II, Reynolds IJ, Dineley KE (2005) Simultaneous detection of intracellular free calcium and zinc using fura-2FF and FluoZin-3. *Cell Calcium* 37:225–232. 10.1016/j.ceca.2004.10.003 [PubMed: 15670869]
- Dineley KE, Malaiyandi LM, Reynolds IJ (2002) A reevaluation of neuronal zinc measurements: artifacts associated with high intracellular dye concentration. *Mol Pharmacol* 62:618–627 [PubMed: 12181438]
- Dineley KE, Devinney MJ, Zeak JA et al. (2008) Glutamate mobilizes [Zn²⁺] through Ca²⁺-dependent reactive oxygen species accumulation. *J Neurochem* 106:2184–2193. 10.1111/j.1471-4159.2008.05536.x [PubMed: 18624907]
- Djordjevic VR, Wallace DR, Schweitzer A et al. (2019) Environmental cadmium exposure and pancreatic cancer: evidence from case control, animal and in vitro studies. *Environ Int* 128:353–361. 10.1016/j.envint.2019.04.048 [PubMed: 31078004]
- Duncan FE, Que EL, Zhang N et al. (2016) The zinc spark is an inorganic signature of human egg activation. *Sci Rep* 6:24737 10.1038/srep24737 [PubMed: 27113677]
- Edwards J, Ackerman C (2016) A review of diabetes mellitus and exposure to the environmental toxicant cadmium with an emphasis on likely mechanisms of action. *Curr Diabetes Rev* 12:252–258. 10.2174/1573399811666150812142922 [PubMed: 26264451]
- El Muayed M, Raja MR, Zhang X et al. (2012) Accumulation of cadmium in insulin-producing β cells. *Islets* 4:405–416. 10.4161/isl.23101 [PubMed: 23466887]
- Greger M, Kabir AH, Landberg T et al. (2016) Silicate reduces cadmium uptake into cells of wheat. *Environ Pollut* 211:90–97. 10.1016/j.envpol.2015.12.027 [PubMed: 26745394]
- Hinkle PM, Osborne ME (1994) Cadmium toxicity in rat pheochromocytoma cells: studies on the mechanism of uptake. *Toxicol Appl Pharmacol* 124:91–98. 10.1006/taap.1994.1012 [PubMed: 7507268]
- Hinkle PM, Shanshala ED, Nelson EJ (1992) Measurement of intracellular cadmium with fluorescent dyes. Further evidence for the role of calcium channels in cadmium uptake. *J Biol Chem* 267:25553–25559 [PubMed: 1281160]
- Hyrz KL, Bownik JM, Goldberg MP (2000) Ionic selectivity of low-affinity ratiometric calcium indicators: mag-Fura-2, Fura-2FF and BTC. *Cell Calcium* 27:75–86. 10.1054/ceca.1999.0092 [PubMed: 10756974]
- Johnson ID (2010) Indicators for Ca²⁺, Mg²⁺, Zn²⁺ and other metal ions In: Johnson I, Spence M (eds) *The molecular probes handbook*, 11th edn. Thermo Fisher Scientific, Waltham, pp 828–882
- Johnson CR, Shrout JD, Fein JB (2018) Visualization and quantification of Cd sorption to bacteria using confocal laser scanning microscopy and Cd-specific fluorescent probes. *Chem Geol* 483:21–30. 10.1016/j.chemgeo.2018.02.020
- Johnson CR, Hopf J, Shrout JD, Fein JB (2019) Testing the component additivity approach to surface complexation modeling using a novel cadmium-specific fluorescent probe technique. *J Colloid Interface Sci* 534:683–694. 10.1016/j.jcis.2018.09.070 [PubMed: 30268085]
- Kay AR, Rumschik SM (2011) Differential transition metal uptake and fluorescent probe localization in hippocampal slices. *Metalomics* 3:829–899. 10.1039/c1mt00024a [PubMed: 21681308]
- Lee W-K, Bork U, Gholamrezaei F, Thévenod F (2005) Cd(2⁺)-induced cytochrome c release in apoptotic proximal tubule cells: role of mitochondrial permeability transition pore and Ca(2⁺) uniporter. *Am J Physiol Renal Physiol* 288:F27–F39. 10.1152/ajprenal.00224.2004 [PubMed: 15339793]

- Li M, Kondo T, Zhao Q-L et al. (2000) Apoptosis induced by cadmium in human lymphoma U937 Cells through Ca²⁺ - calpain and caspase-mitochondria- dependent pathways. *J Biol Chem* 275:39702–39709. 10.1074/jbc.M007369200 [PubMed: 10970901]
- Li D, Chen S, Bellomo EA et al. (2011) Imaging dynamic insulin release using a fluorescent zinc indicator for monitoring induced exocytotic release (ZIMIR). *Proc Natl Acad Sci USA* 108:21063–21068. 10.1073/pnas.1109773109 [PubMed: 22160693]
- Malaiyandi LM, Sharthiya H, Dineley KE (2016) Fluorescence detection of intracellular cadmium with Leadmium Green. *Biomaterials* 29:625–635. 10.1007/s10534-016-9939-z [PubMed: 27260023]
- Manzano JI, García-Hernández R, Castanys S, Gamarro F (2013) A new ABC half-transporter in *Leishmania major* is involved in resistance to antimony. *Antimicrob Agents Chemother* 57:3719–3730. 10.1128/AAC.00211-13 [PubMed: 23716044]
- Maxchelator. University of California, Davis <https://somapp.ucdmc.ucdavis.edu/pharmacology/-bers/maxchelator/webmaxc/webmaxcS.htm>. Accessed 18 July 2019
- Miura S, Takahashi K, Imagawa T et al. (2013) Involvement of TRPA1 activation in acute pain induced by cadmium in mice. *Mol Pain* 9:7 10.1186/1744-8069-9-7 [PubMed: 23448290]
- Nordberg GF (2009) Historical perspectives on cadmium toxicology. *Toxicol Appl Pharmacol* 238:192–200. 10.1016/j.taap.2009.03.015 [PubMed: 19341754]
- Ortega P, Custódio MR, Zanotto FP (2017a) Characterization of cadmium transport in hepatopancreatic cells of a mangrove crab *Ucides cordatus*: the role of calcium. *Aquat Toxicol* 188:92–99. 10.1016/j.aquatox.2017.04.012 [PubMed: 28475951]
- Ortega P, Vitorino HA, Moreira RG et al. (2017b) Physiological differences in the crab *Ucides cordatus* from two populations inhabiting mangroves with different levels of cadmium contamination. *Environ Toxicol Chem* 36:361–371. 10.1002/etc.3537 [PubMed: 27329273]
- Romero D, Hernández-García A, Tagliati CA et al. (2009) Cadmium- and lead-induced apoptosis in mallard erythrocytes (*Anas platyrhynchos*). *Ecotoxicol Environ Saf* 72:37–44. 10.1016/j.ecoenv.2008.05.004 [PubMed: 18579205]
- Shibuya I, Douglas WW (1992) Calcium channels in rat melanotrophs are permeable to manganese, cobalt, cadmium, and lanthanum, but not to nickel: evidence provided by fluorescence changes in fura-2-loaded cells. *Endocrinology* 131:1936–1941. 10.1210/endo.131.4.1327724 [PubMed: 1327724]
- Soibinet M, Souchon V, Leray I, Valeur B (2008) Rhod-5N as a fluorescent molecular sensor of cadmium(II) ion. *J Fluoresc* 18:1077–1082. 10.1007/s10895-008-0352-z [PubMed: 18488146]
- Taki M (2013) Imaging and sensing of cadmium in cells In: Sigel A, Sigel H, Sigel RKO (eds) *Cadmium: from toxicity to essentiality*. Springer, Dordrecht, pp 99–115
- Thévenod F (2010) Catch me if you can! Novel aspects of cadmium transport in mammalian cells. *Biomaterials* 23:857–875. 10.1007/s10534-010-9309-1 [PubMed: 20204475]
- Usai C, Barberis A, Moccagatta L, Marchetti C (1999) Pathways of cadmium influx in mammalian neurons. *J Neurochem* 72:2154–2161. 10.1046/j.1471-4159.1999.0722154.x [PubMed: 10217297]
- Vinkenborg JL, van Duijnhoven SMJ, Merckx M (2011) Reengineering of a fluorescent zinc sensor protein yields the first genetically encoded cadmium probe. *Chem Commun* 47:11879–11883. 10.1039/c1cc14944j
- Vo-Dinh T, Viallet P, Ramirez L et al. (1994) Detection of cadmium ion using the fluorescence probe Indo-1. *Anal Chim Acta*. 10.1016/0003-2670(94)80335-8
- Zanella L, Fattorini L, Brunetti P et al. (2015) Overexpression of AtPCS1 in tobacco increases arsenic and arsenic plus cadmium accumulation and detoxification. *Planta* 243:605–622. 10.1007/s00425-015-2428-8 [PubMed: 26563149]
- Zhao J, Bertoglio BA, Devinney MJ et al. (2009) The interaction of biological and noxious transition metals with the zinc probes FluoZin-3 and Newport Green. *Anal Biochem* 384:34–41 [PubMed: 18848515]
- Zhou J, Li W, Xie Q et al. (2014) Research article effects of simvastatin on glucose metabolism in mouse MIN6 cells. *J Diabetes Res*. 10.1155/2014/376570

**Fig. 1.**

Summary of ratiometric (a) or single wavelength (d) dye responses to 5-min depolarizing stimulus supplemented with CdCl₂ (30 μM). Bars represent mean ± SD change in (a) fluorescence ratio or (d) F/F₀. These trials were carried out in nominally Ca²⁺-free buffer. Representative fluorescence micrographs before and after 30 μM CdCl₂ and depolarization, for fura-2 (b, c) or FluoZin-3 (e, f). F2 fura-2, F2FF Fura-2FF, Indo Indo-1, MF2 mag-fura-2, F5N Fluo-5N, FZ1 FluoZin-1, FZ2 FluoZin-2, FZ3 FluoZin-3, LG Leadmium Green, NG Newport Green DCF, R5N Rhod-5N, CG5N Calcium Green-5N. Time stamp is in minute:second format

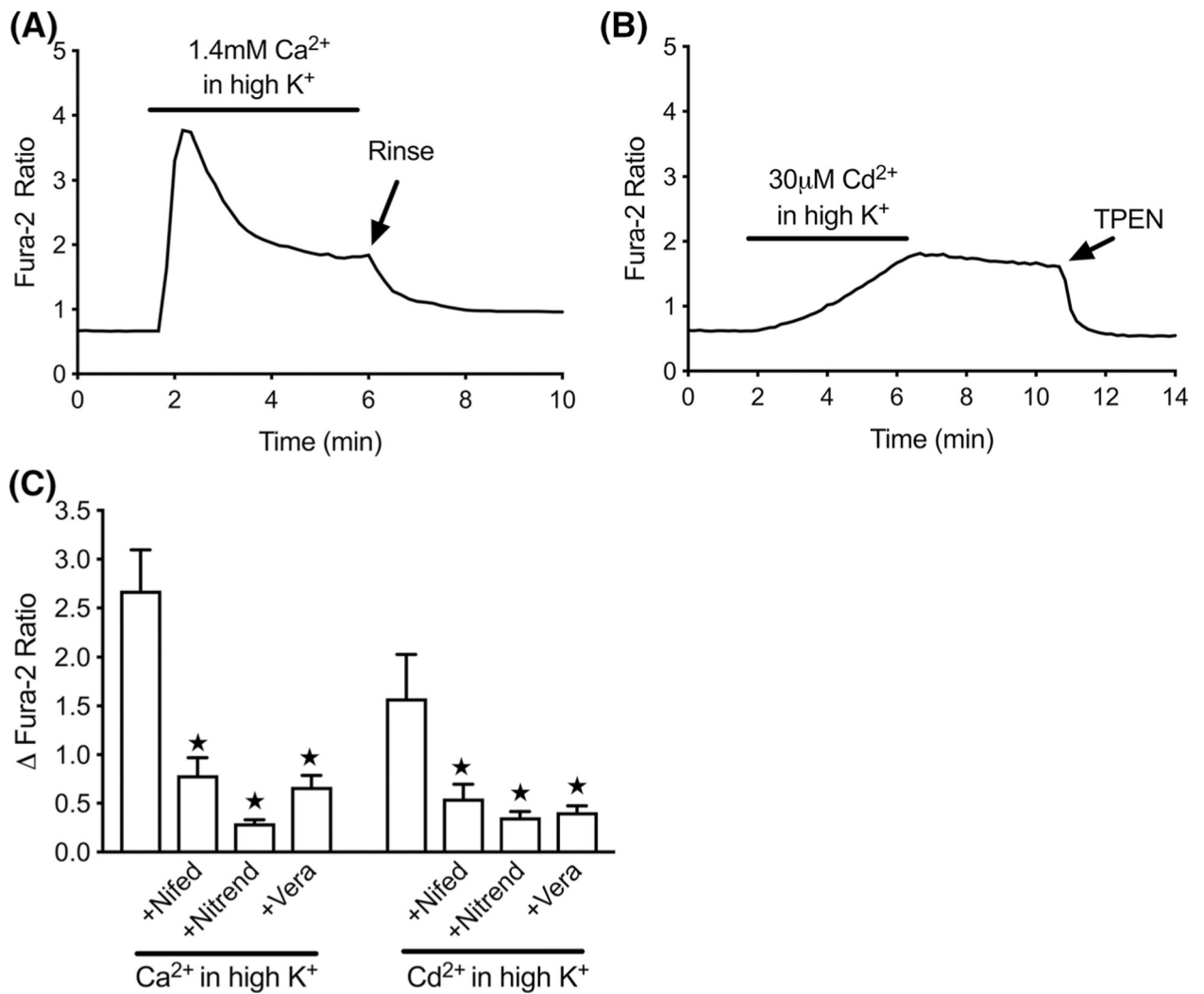


Fig. 2. Comparison of fura-2 detection of depolarization-induced $[Ca^{2+}]_i$ and $[Cd^{2+}]_i$ accumulation. **a** Representative fura-2 response to depolarization for 5 min in the presence of $CaCl_2$ (1.4 mM), followed by HBSS rinse. **b** Representative fura-2 response to depolarization for 5 min in the presence of $CdCl_2$ (30 μ M), followed by 5 min rinse, then TPEN (50 μ M). **c** Summary data for VGCC inhibition of fura-2 response to depolarization-induced accumulation of $[Ca^{2+}]_i$ or $[Cd^{2+}]_i$. For experiments with VGCC blockers, cells were pretreated for 3 min with 1 μ M nifedipine, nitrendipine, or verapamil prior to depolarization stimulus. All Cd^{2+} trials were performed in nominally Ca^{2+} -free buffer. Bars represent mean \pm SD fura-2 ratio change. $\star p < 0.05$ using Welch's t-test

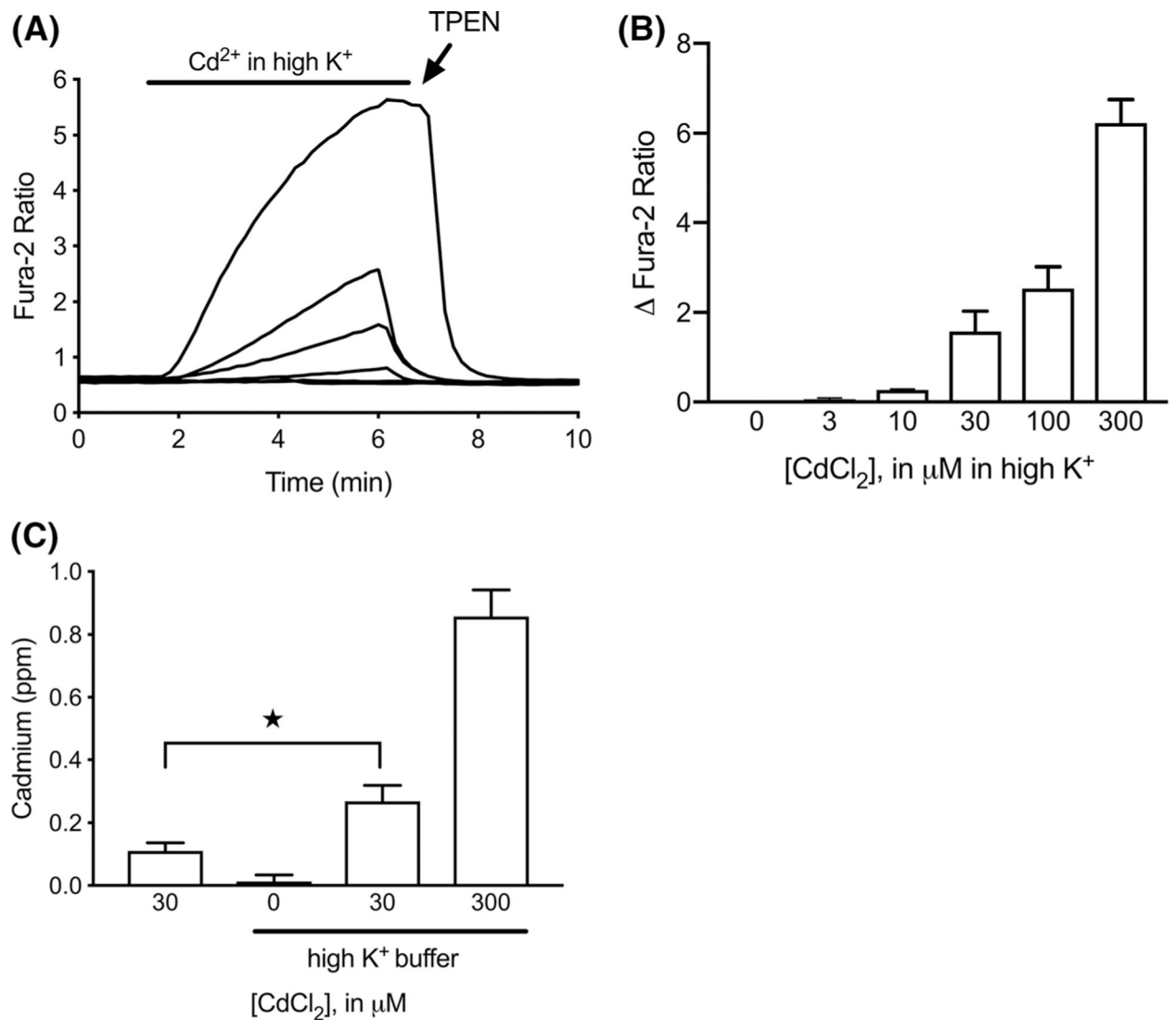


Fig. 3. Fura-2 concentration-dependent response to depolarization-induced $[\text{Cd}^{2+}]_i$ accumulation. **a** Representative traces from cells depolarized for 5 min in the presence of CdCl_2 (0, 3, 10, 30, 100, and 300 μM), then treated with 50 μM TPEN. **b** Summary of peak fura-2 ratio changes from experiments in **a**. **c** ICP-MS measurements of Cd^{2+} accumulation in MIN6 cells. Bars represent mean \pm SD ratio change. These trials were carried out in nominally Ca^{2+} -free buffer. $\star p < 0.05$ using one-way ANOVA with Tukey's multiple comparisons test

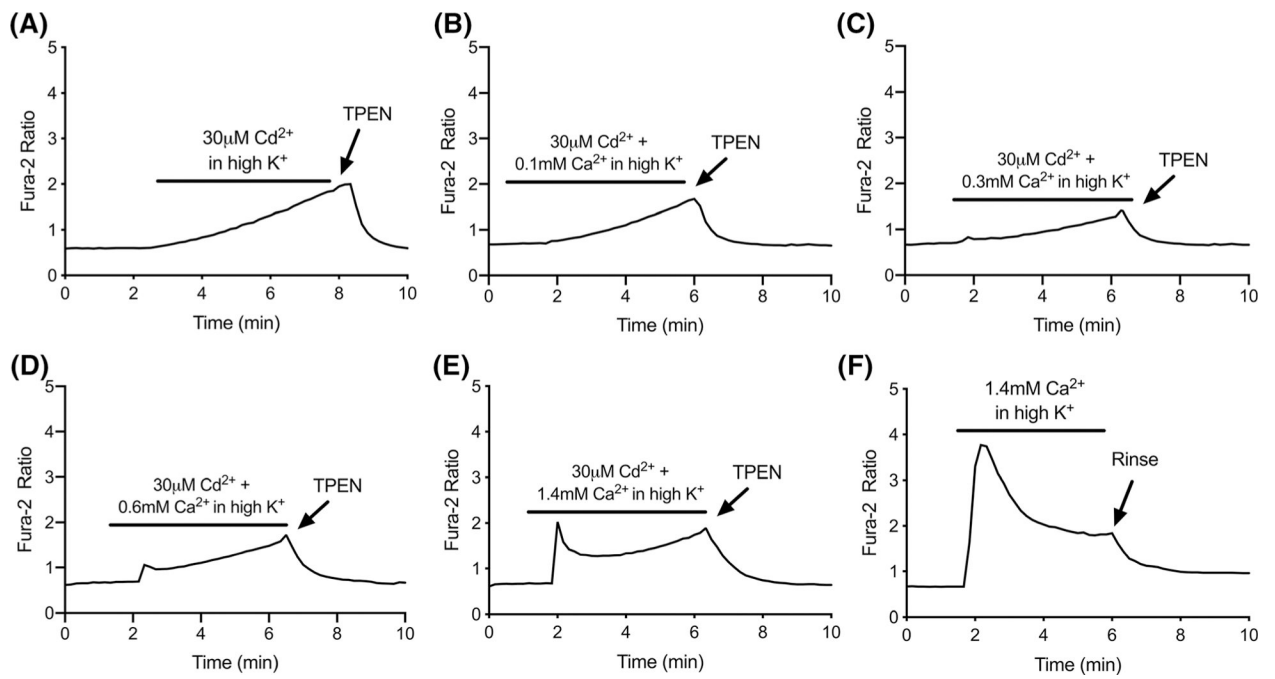


Fig. 4.

Representative traces of fura-2 response to depolarization-induced $[Cd^{2+}]_i$ accumulation in the presence of extracellular Ca^{2+} . **a–e** Cells were depolarized for 5 min in the presence of $CdCl_2$ (30 μM), and varying extracellular $CaCl_2$ (0, 0.1, 0.3, 0.6, and 1.4 mM). **f** For comparison, representative trace of fura-2 response to $CaCl_2$ (1.4 mM) in depolarizing conditions without $CdCl_2$

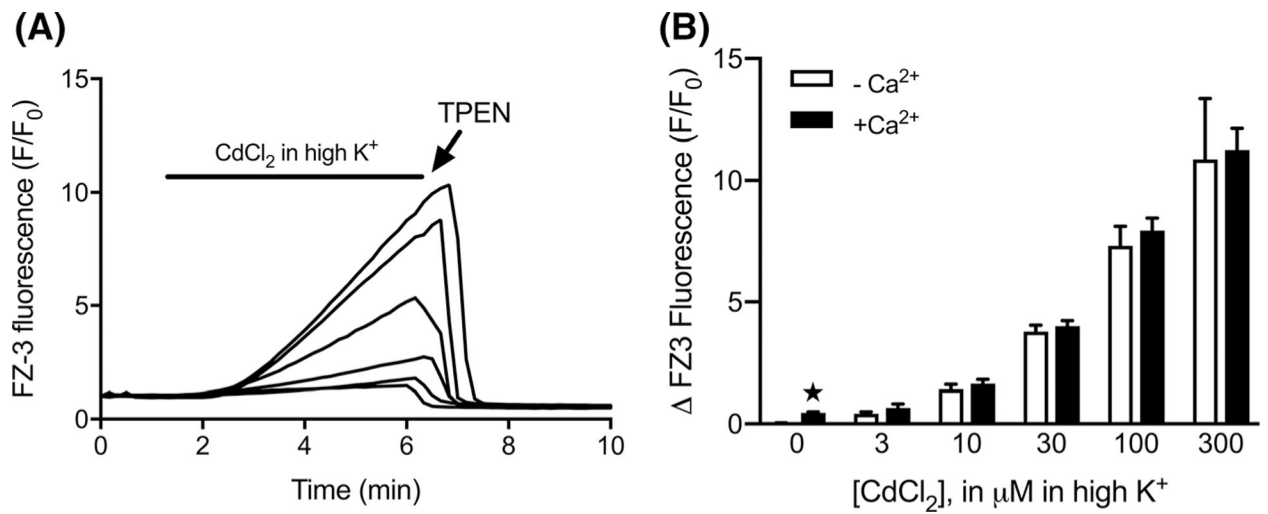


Fig. 5. FluoZin-3 response to depolarization-induced $[Cd^{2+}]_i$ accumulation amidst physiological extracellular Ca^{2+} . **a** Representative traces of cells depolarized for 5 min in the presence of $CdCl_2$ (0, 3, 10, 30, 100 and 300 μM) and 1.4 mM $CaCl_2$, then treated with 50 μM TPEN. **b** Comparison of peak fluorescence induced by $[Cd^{2+}]_i$ in the presence (solid) and absence (open) of 1.4 mM extracellular Ca^{2+} . Bars represent mean \pm SD FluoZin-3 F/F_0 change. ★ $p < 0.05$ using Welch's t-test

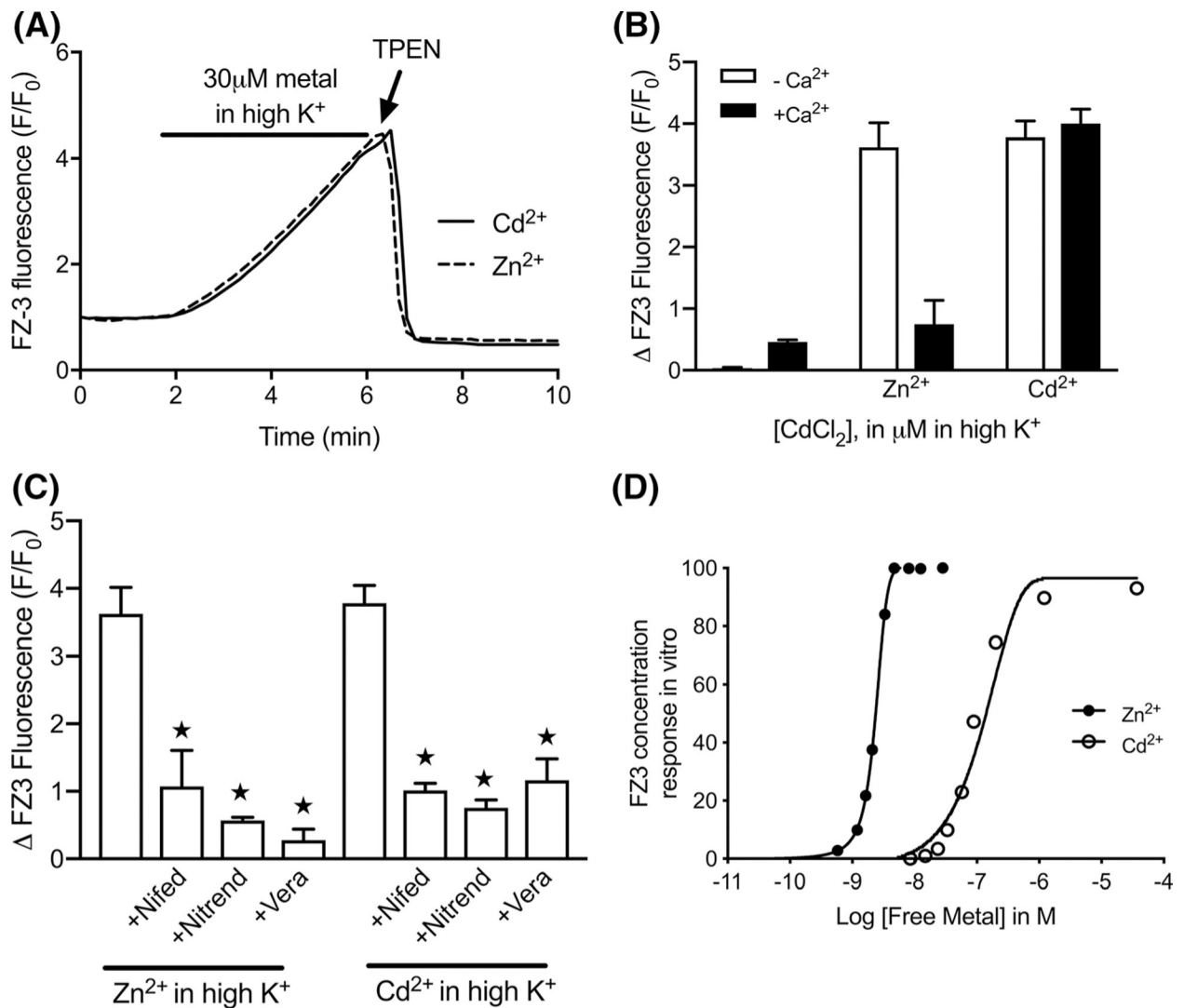


Fig. 6. Comparison of FluoZin-3 detection of depolarization-induced accumulation of $[\text{Cd}^{2+}]_i$ and $[\text{Zn}^{2+}]_i$. **a** Representative traces of cells depolarized for 5 min in the presence of 30 μM CdCl_2 (solid line) or 30 μM ZnSO_4 (dashed line), then treated with 50 μM TPEN. **b** Peak fluorescence induced by $[\text{Zn}^{2+}]_i$ or $[\text{Cd}^{2+}]_i$ in the absence (open bars) or presence (solid bars) of 1.4 mM extracellular CaCl_2 in depolarizing conditions. **c** Summary data for VGCC inhibition of FluoZin-3 changes in response to depolarization-induced $[\text{Zn}^{2+}]_i$ or $[\text{Cd}^{2+}]_i$ accumulation. For experiments with VGCC blockers, cells were pretreated for 3 min with 1 μM nifedipine, nitrendipine, or verapamil prior to depolarization stimulus. Trials in **a**, **c** were carried out in nominally Ca^{2+} -free buffer. Bars represent mean \pm SD FluoZin-3 F/F_0 change; $\star p < 0.05$ using Welch's t-test. **d** In vitro comparisons of FluoZin-3 response to Cd^{2+} (open) and Zn^{2+} (solid). FluoZin-3 fluorescence was measured in the presence of free Cd^{2+} (0 – 3.69×10^{-5} M; open) or Zn^{2+} (0 – 2.82×10^{-8} M; solid). Fluorescence was expressed as percent of maximal fluorescence achieved with Zn^{2+} . Calculated dissociation constants, K_D , for Zn^{2+} and Cd^{2+} are 3.67 nM and 129 nM, respectively

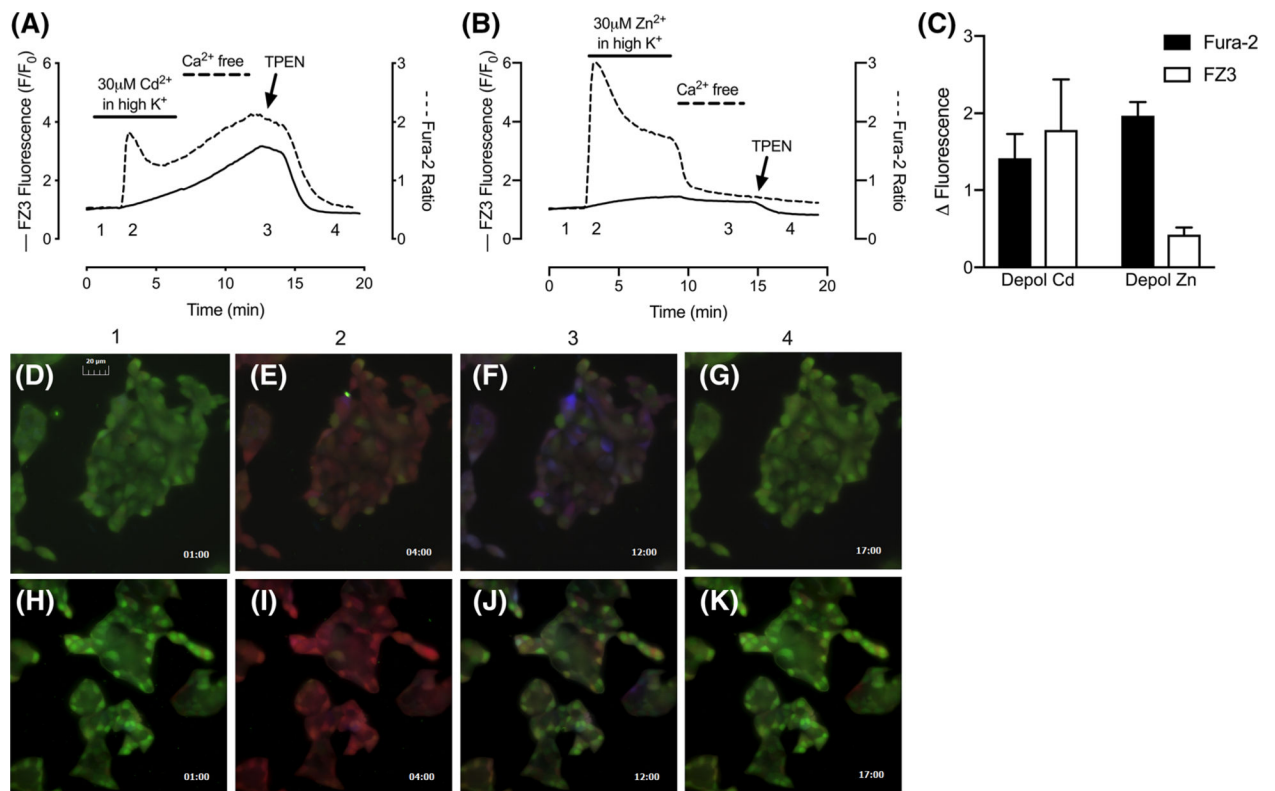
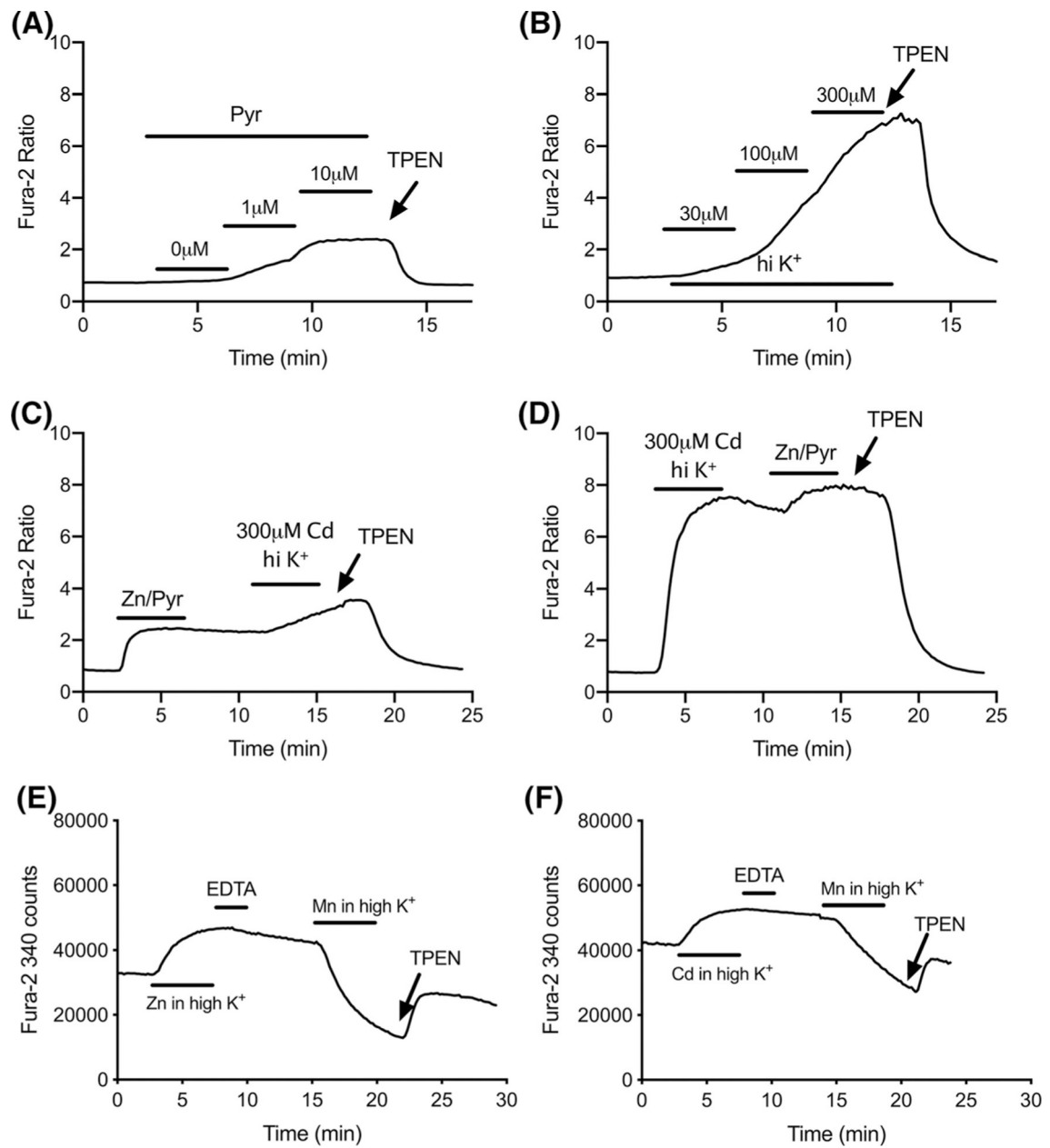


Fig. 7. Simultaneous monitoring of $[Cd^{2+}]_i$ and $[Ca^{2+}]_i$, or $[Zn^{2+}]_i$ and $[Ca^{2+}]_i$ with dual dye approach. **a** Representative fura-2 and FluoZin-3 traces recorded from cells co-loaded with both dyes and depolarized for 5 min in the presence of 1.4 mM $CaCl_2$ and 30 μM $CdCl_2$, rinsed with Ca^{2+} -free buffer for 5 min, then treated with 50 μM TPEN. Left axis corresponds to FluoZin-3 F/F_0 (solid line); right axis corresponds to fura-2 ratio (dotted line). **b** Same paradigm as in **a**, but with 30 μM $ZnSO_4$ instead of $CdCl_2$. **c** Summary changes (mean \pm SD) in fura-2 ratio (solid bars) or FluoZin-3 F/F_0 (open bars) in response to Cd^{2+} or Zn^{2+} under depolarizing conditions. **d–k.** Composite fluorescence micrographs of fura-2 and FluoZin-3 in response to $[Cd^{2+}]_i$ and $[Ca^{2+}]_i$ (**d–g**), or $[Zn^{2+}]_i$ and $[Ca^{2+}]_i$ (**h–k**). Micrographs correspond to timepoints 1–4 indicated on the representative traces: 1 (**d, h**), 2 (**e, i**), 3 (**f, j**) and 4 (**g, k**). Time stamp in minute:second format

**Fig. 8.**

Using fura-2 to distinguish between $[\text{Zn}^{2+}]_i$ and $[\text{Cd}^{2+}]_i$. **a** Representative fura-2 traces recorded from cells treated for 3-min sequential additions of 20 μM sodium pyrithione in the presence of 0, 1 and 10 μM ZnSO₄, and reversed with 50 μM TPEN. **b** Representative fura-2 traces recorded from cells treated sequentially for 3 min each with 30, 100 and 300 μM CdCl₂ in the presence of depolarizing buffer, then reversed with 50 μM TPEN. **c** Representative fura-2 trace of cells treated for 5 min with 10 μM ZnSO₄ and 20 μM sodium pyrithione, followed by 3 min rinse, then 5 min of 300 μM CdCl₂ in the presence of depolarizing buffer. **d** Representative fura-2 trace from cells treated for 5 min with 300 μM CdCl₂ in the presence of depolarizing buffer, followed by 3 min rinse then 5 min of 20 μM sodium pyrithione with 10 μM ZnSO₄. Experiments were terminated with 50 μM TPEN.

Fura-2 counts at 340 nm from cells treated with either 50 μM ZnSO_4 (e) or CdCl_2 (f) in high KCl buffer for 5 min, followed by 50 μM EDTA, then rinsed with regular buffer, treated with 50 μM MnCl_2 in high KCl buffer, and finally reversed with 50 μM TPEN

Author Manuscript

Author Manuscript

Author Manuscript

Author Manuscript